$PtSe_2$ Field-Effect Transistors: New Opportunities for Electronic Devices

AbdulAziz AlMutairi, Demin Yin, and Youngki Yoon, *Member, IEEE*

***Abstract*— $PtSe_2$, a new family of transition metal dichalcogenides, has been explored for electronic device applications using density functional theory (DFT) and non-equilibrium Green's function (NEGF) within the third nearest neighbor tight-binding approximation. Interestingly, despite its small effective mass (m_e* as low as 0.21m_0; m_0 being electron rest mass), $PtSe_2$ has large density of states (DOS) due to its unique six-valley conduction band within the first Brillouin zone, unlike MoX_2 family. This has direct impacts on the device characteristics of $PtSe_2$ field-effect transistors, resulting in superior on-state performance (30% higher on current and transconductance) as compared to the $MoSe_2$ counterpart. Our simulation shows that $PtSe_2$ device with a channel longer than 15 nm exhibits near-ideal subthreshold swing, and sub-100 mV/V of drain-induced barrier lowering can be achieved with an aggressively scaled gate oxide, demonstrating new opportunities for electronic devices with novel $PtSe_2$.**

***Index Terms*—$PtSe_2$, Field-Effect Transistors, Quantum Transport, Non-Equilibrium Green's Function**

I. Introduction

Transition metal dichalcogenides (TMDs) have been the center of attention among two-dimensional (2D) materials for various applications such as electronic and optoelectronic devices as well as sensors due to their suitable bandgap, excellent electrical and optical properties, and mechanical stability [1], [2]. Among TMDs, the group-VIB transition metal dichalcogenides such as MoX_2 and WX_2 (X = S, Se, Te) have been studied extensively [3]–[6]. Recently, a new family of TMDs, namely PtX_2, based on group-10 transition metal has emerged [7], [8]. Platinum diselenide ($PtSe_2$) has been synthesized using direct deposition of Se atoms on a Pt substrate [7], and it was predicted that $PtSe_2$ has the highest mobility among PtX_2 family [8]–[10]. PtX_2 family favors 1T crystal structure, unlike MoX_2 and WX_2 in which 2H structure is known to be stable (Figs. 1(a) and (b)). In addition, bulk PtX_2 is metallic in nature which is not the case of MoX_2 and WX_2 [8].

In this study, we for the first time investigate the potential and the ultimate performance limit of monolayer $PtSe_2$ field-effect transistors (FETs) using atomistic quantum transport simulations. To do this, we calculate the electronic states of $PtSe_2$ using density functional theory (DFT), from which tight-binding parameters are extracted for non-equilibrium Green's function (NEGF) device simulation. Transfer characteristics of $PtSe_2$ devices are investigated, and the on and off-state characteristics are thoroughly examined by scaling channel length and equivalent oxide thickness (EOT). Moreover, the performance of $PtSe_2$ FET is compared with its 2H-$MoSe_2$ counterpart, and the superior on-state characteristics of $PtSe_2$ are discussed based on the unique material properties of 1T-PtX_2 family.

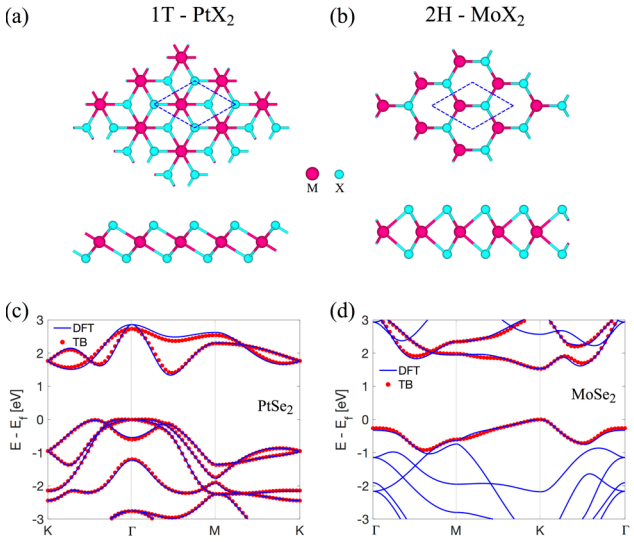

Fig. 1. (a) 1T-PtX_2 (X = Se, S, Te) and (b) 2H-MoX_2 crystalline structure. (Top panel) top view; (bottom) side view. M represents Pt or Mo atom. Dashed diamonds illustrate unit cells. Density functional theory (DFT) band structures for monolayer (c) $PtSe_2$ and (d) $MoSe_2$ (blue solid lines). Third nearest neighbour tight-binding (TB) band structures are also shown in (c) and (d) with red dots, exhibiting excellent matching with the DFT bands.

II. Simulation Method

Electronic states are calculated based on plane wave DFT calculations using Quantum ESPRESSO [11] with generalized gradient approximation (GGA) and projector augmented wave (PAW) pseudopotential. The kinetic energy cutoff of the wavefunction is 50 Ry. The structures are relaxed until the total force becomes less than 0.001 Ry/a.u. and the stress is less than 10^{-7} Ry/a_0^3 (a_0 being bohr) in all directions. The unit cell contains one M atom (Pt, Mo) and two Se atoms (dashed diamond in Figs. 1(a) and (b)). The band structures are plotted along the high symmetry points of the first Brillouin zone (BZ) in Figs. 1(c) and (d).

This work was supported in part by NSERC Discovery Grant (RGPIN-05920-2014) and in part by NSERC Strategic Project Grant (STPGP 478974-15). Computing resources were provided by Calcul Quebec through Compute Canada. AbdulAziz AlMutairi and Demin Yin acknowledge the financial support by WIN Nanofellowship.

The authors are with Department of Electrical and Computer Engineering & Waterloo Institute for Nanotechnology at the University of Waterloo, Waterloo, ON, Canada N2L 3G1 (Email: youngki.yoon@uwaterloo.ca).

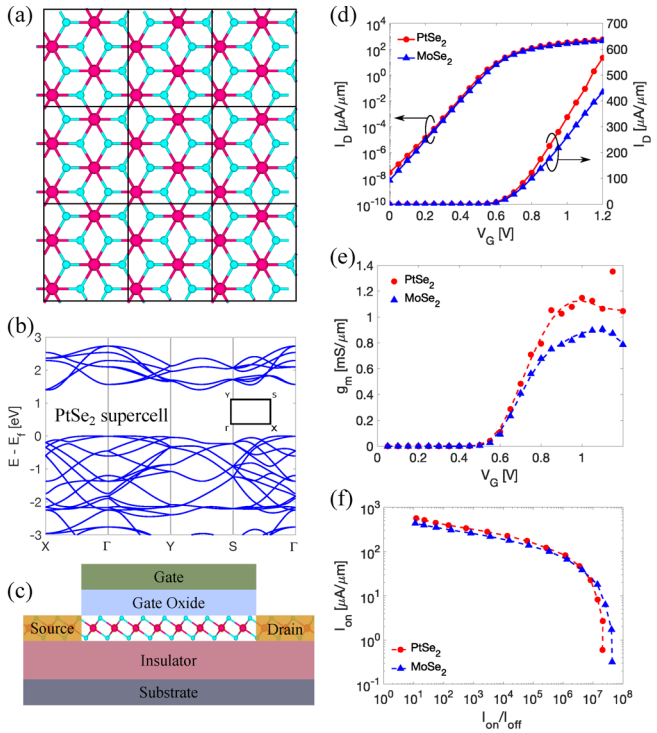

Fig. 2. (a) Nine supercells of $PtSe_2$ chosen for NEGF device simulations. Solid black box shows one supercell, which includes four unit cells of $PtSe_2$. (b) Band structure of the supercell where the transport direction is in Γ→X, which is equivalent to Γ→M direction for the unit cell. (Inset) The high symmetry points of the supercell. (c) Simulated device structure. (d) Transfer characteristics, (e) transconductance, g_m vs. V_G, and (f) I_{on} vs. I_{on}/I_{off} of $PtSe_2$ and $MoSe_2$ FETs.

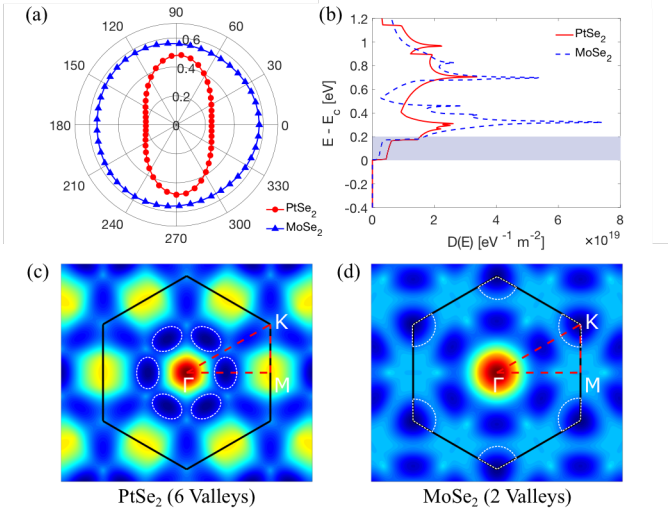

Fig. 3. (a) Polar plot of effective mass for electrons (m_e*) for $PtSe_2$ and $MoSe_2$. $PtSe_2$ exhibits significant anisotropic effective mass near E_c, unlike $MoSe_2$. 0° represents Γ→M direction for $PtSe_2$; K→ Γ for $MoSe_2$. (b) Density of states (DOS) per spin in the conduction band of $PtSe_2$ and $MoSe_2$. Notably, $PtSe_2$ exhibits larger DOS than $MoSe_2$ near the bottom of the conduction band ($E - E_c < 0.2$ eV), which is the most relevant energy range for electron transport. Surface plot of the conduction band edge in k-space for (c) $PtSe_2$ and (d) $MoSe_2$. The first Brillouin zone (BZ) is shown with hexagons (black solid lines) and the irreducible BZ with triangles (red dashed lines).

To preform device simulations, input material parameters are required. Unlike $MoSe_2$, tight-binding (TB) parameters for $PtSe_2$ have not been reported yet, and therefore, we have created TB parameters. For this, maximum localized Wannier function (MWLF) approach has been employed using Wannier90 [12]. Wannierization was done using 11 initial projections reflecting five *d*-orbitals of Pt atom and three *p*-orbitals of Se atom. The TB parameters of $MoSe_2$ were adopted from a previous report [13]. For both materials, third nearest neighbor TB parameters have been used since it can provide a high level of accuracy, and at the same time, it is computationally manageable. The parameters exhibit excellent matching to the DFT results as shown in Figs. 1(c) and (d).

To assess the carrier transport in FETs based on these two materials, NEGF method within a tight-binding approximation has been utilized. The transport equation was solved self-consistently with Poisson's equation [14]. Ballistic transport is assumed due to the relatively short channel length considered in this study. Periodic boundary condition is used in the transverse direction with 400 k_y sampling points (k_y being the wavenumber in the transverse direction). A rectangular supercell shown in Fig. 2(a) has been chosen to construct the Hamiltonian matrix (H) for the sake of simplicity. X (transport) direction is chosen to be equivalent to Γ→M direction for the unit cell; Y (transverse) direction is perpendicular to it. The band structure of the $PtSe_2$ supercell is shown in Fig. 2(b). On the other hand, for $MoSe_2$, transport direction is defined in K→Γ following previous studies [3]. The simulated device structure is shown in Fig. 2(c) and parameters for a nominal device are as follows: channel length L_{ch} = 15 nm; Al_2O_3 (dielectric constant κ = 9) gate dielectric thickness t_{ox} = 2.5 nm; source/drain doping concentration of 1.5×10^{13} cm^{-2}; power supply voltage V_{DD} = 0.5 V.

III. Results

As shown in Fig. 1(c), $PtSe_2$ exhibits conduction band minimum (E_c) between Γ and M points, whereas $MoSe_2$ has its minimum at K point (Fig. 1(d)). The electron effective mass m_e* of $PtSe_2$ (0.21 m_0) is smaller than that of $MoSe_2$ (0.56 m_0). In contrary to the case of $MoSe_2$, $PtSe_2$ exhibits significant anisotropic effective mass for electrons as shown in Fig. 3(a).

Figure 2(d) shows the transfer characteristic of $PtSe_2$ FET, which is compared with $MoSe_2$ counterpart. While both devices show near-identical off-state characteristics with subthreshold swing (SS = $\partial V_G/\partial log_{10}(I_D)$; V_G and I_D are gate voltage and drain current, respectively) of ~64 mV/dec, on-state characteristics of $PtSe_2$ surpass that of $MoSe_2$, resulting in 30% higher on current (I_{on}) and transconductance ($g_m = \partial I_D/\partial V_G$) as shown in Figs. 2(d) and 2(e). The overall performance of the device can be evaluated by plotting I_{on} vs. on/off current ratio (I_{on}/I_{off}) as shown in Fig. 2(f), where $PtSe_2$ shows superior performance than $MoSe_2$. For instance, at a common I_{on} of 250 μA/μm, I_{on}/I_{off} of $PtSe_2$ is 6.7×10^3, which is ~5 times larger than that of $MoSe_2$ (1.4×10^3). In addition, for a common I_{on}/I_{off} of 10^4, $PtSe_2$ shows I_{on} = 236 μA/μm, which is 25% greater than the $MoSe_2$ value.

The superior on-state characteristics of $PtSe_2$ result mainly from its large density of states (DOS). In contrary to the general belief that smaller effective mass leads to lower DOS, $PtSe_2$ with relatively small effective mass has larger DOS than $MoSe_2$. This is attributed to the fact that $PtSe_2$ has six conduction band valleys within the first BZ, whereas $MoSe_2$

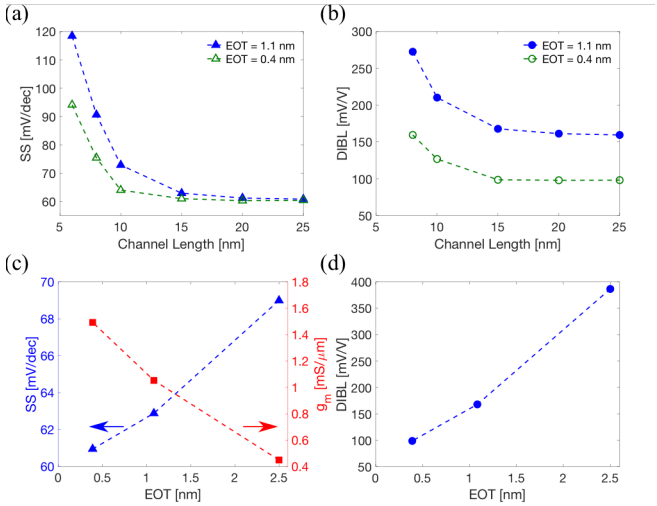

Fig. 4. (a) Subthreshold swing (SS) and (b) drain-induced barrier lowering (DIBL) of $PtSe_2$ FETs for L_{ch} = 6–25 nm with EOTs of 1.1 nm (filled markers) and 0.4 nm (open markers). (c) SS (blue triangles) and g_m (red squares) and (d) DIBL as a function of EOT (with L_{ch} = 15 nm) for $PtSe_2$ FETs.

has only two valleys as clearly seen in Figs. 3(c) and 3(d). Therefore, $PtSe_2$ has higher DOS than $MoSe_2$ near the conduction band edge ($E - E_c < 0.2$ eV) as shown in Fig. 3(b). Notably, this is the energy range of interest for electron transport. Although $MoSe_2$ has higher DOS at the energy range of 0.2 eV < $E - E_c$ < 0.4 eV, it has only negligible contribution to the current flow. It should be noted that having six valleys in the conduction band may increase the possibility of intervalley scattering, which can result in current degradation to some extent. However, the detailed investigation of the effect of scattering is beyond the scope of this study.

In general, 2D material devices are known for their high immunity to short-channel effect (SCE). However, due to the unique electronic properties of $PtSe_2$, a careful investigation should be given. Thus, we explore the effect of channel length scaling on SS and drain-induced barrier lowering (DIBL = $\Delta V_{TH}/\Delta V_D$; ΔV_{TH} and ΔV_D being the changes in threshold voltage and drain voltage, respectively) by varying L_{ch} from 6 to 25 nm with a nominal EOT of 1.1 nm. Figure 4(a) shows that SS is close to the theoretical limit of 60 mV/dec for $L_{ch} \geq 15$ nm. However, with sub-10 nm channel, it exhibits significant degradation, leading to 91 mV/dec in case of L_{ch} = 8 nm, which is similar to that of $MoSe_2$ device (89 mV/dec). DIBL also shows a similar trend as SS as it can be seen in Fig. 4(b). With a nominal EOT, DIBL is 160 mV/V for $L_{ch} \geq 15$ nm, while it increases to 270 mV/V at L_{ch} = 8 nm, which is larger than that of $MoSe_2$ device (200 mV/V) at the same channel length. Nonetheless, both SS and DIBL of $PtSe_2$ FET can be improved by using thinner EOT, particularly for short-channel devices, as discussed next.

Finally, we have done an EOT scaling study to further engineer device performance of $PtSe_2$ FETs. Besides the nominal EOT (2.5 nm-thick Al_2O_3), we have adopted one thicker (SiO_2; κ = 3.9) and one thinner EOT (HfO_2; κ = 25). Figure 4(c) shows that, with an EOT of 0.4 nm, SS can be as low as 61 mV/dec and g_m can be as large as 1.49 mS/μm with L_{ch} = 15 nm. In addition, sub-100 mV/V DIBL can be achievable with the reduced EOT (Fig. 4(d)), allowing further optimization of novel $PtSe_2$ device performance. Notably, the scaling of EOT can significantly suppress the SCE as it can be seen in Figs. 4(a) and (b) (open markers).

IV. Conclusion

Material properties and device characteristics of a new TMD family of $PtSe_2$ have been studied. Electronic band structures are plotted using DFT, from which third nearest neighbor TB parameters are extracted for NEGF device simulations. DFT results reveal that 1T-PtX_2 has the conduction band minima between Γ and M points, thereby forming six conduction band valleys within the first BZ, unlike 2H-MoX_2. Therefore, $PtSe_2$ exhibits significantly larger DOS near the E_c despite relatively small effective mass, compared to $MoSe_2$. This allows it to have superior on-state characteristics (I_{on} and g_m) as compared with the $MoSe_2$ counterpart. We also performed a scaling study by varying L_{ch} and EOT. Despite the fact that short-channel effect has been observed, it can be suppressed significantly with a channel longer than 15 nm or an EOT less than 1 nm. Although significant anisotropic effective mass is observed within each conduction band valley, it is expected that current level would remain almost same for both armchair and zigzag directions, since the total current is determined by the overall contribution from the six valleys with rotational symmetry, which is in agreement with experiment [8].

References

[1] H. L. Zhuang and R. G. Hennig, "Computational Search for Single-Layer Transition-Metal Dichalcogenide Photocatalysts," *J. Phys. Chem. C*, vol. 117, no. 40, pp. 20440–20445, 2013. doi:10.1021/jp405808a.

[2] F. A. Rasmussen and K. S. Thygesen, "Computational 2D Materials Database: Electronic Structure of Transition-Metal Dichalcogenides and Oxides," *J. Phys. Chem. C*, vol. 119, no. 23, pp. 13169–13183, 2015. doi:10.1021/acs.jpcc.5b02950.

[3] Y. Yoon, K. Ganapathi, and S. Salahuddin, "How good can monolayer MoS_2 transistors be?," *Nano Lett.*, vol. 11, no. 9, pp. 3768–3773, 2011. doi:10.1021/nl2018178.

[4] J. Kwon, Y. K. Hong, G. Han, I. Omkaram, W. Choi, S. Kim, and Y. Yoon, "Giant Photoamplification in Indirect-Bandgap Multilayer MoS_2 Phototransistors with Local Bottom-Gate Structures," *Adv. Mater.*, vol. 27, no. 13, pp. 2224–2230, 2015. doi:10.1002/adma.201404367.

[5] S. B. Desai, S. R. Madhvapathy, A. B. Sachid, J. P. Llinas, Q. Wang, G. H. Ahn, G. Pitner, M. J. Kim, J. Bokor, C. Hu, A. Javey, H.-S. P. Wong, and A. Javey, "MoS_2 transistors with 1-nanometer gate lengths," *Science.*, vol. 354, no. 6308, pp. 99–102, 2016. doi:10.1126/science.aah4698.

[6] S. Wachter, D. K. Polyushkin, O. Bethge, and T. Mueller, "A microprocessor based on a two-dimensional semiconductor," *Nat. Commun.*, vol. 8, p. 14948, 2017. doi:10.1038/ncomms14948.

[7] Y. Wang, L. Li, W. Yao, S. Song, J. T. Sun, J. Pan, X. Ren, C. Li, E. Okunishi, Y. Q. Wang, E. Wang, Y. Shao, Y. Y. Zhang, H. T. Yang, E. F. Schwier, H. Iwasawa, K. Shimada, M. Taniguchi, Z. Cheng, S. Zhou, S. Du, S. J. Pennycook, S. T. Pantelides, and H. J. Gao, "Monolayer $PtSe_2$, a New Semiconducting Transition-Metal-Dichalcogenide, Epitaxially Grown by Direct Selenization of Pt," *Nano Lett.*, vol. 15, no. 6, pp. 4013–4018, 2015. doi:10.1021/acs.nanolett.5b00964.

[8] Y. Zhao, J. Qiao, Z. Yu, P. Yu, K. Xu, S. P. Lau, W. Zhou, Z. Liu, X. Wang, W. Ji, and Y. Chai, "High-Electron-Mobility and Air-Stable 2D Layered $PtSe_2$ FETs," *Adv. Mater.*, vol. 1604230, 2016. doi:10.1002/adma.201604230.

[9] W. Zhang, Z. Huang, W. Zhang, and Y. Li, "Two-dimensional semiconductors with possible high room temperature mobility,"

Nano Res., vol. 7, no. 12, pp. 1731–1737, 2014. doi: 10.1007/s12274-014-0532-x.

[10] Y. Zhao, J. Qiao, P. Yu, Z. Hu, Z. Lin, S. P. Lau, Z. Liu, W. Ji, and Y. Chai, "Extraordinarily Strong Interlayer Interaction in 2D Layered PtS_2," *Adv. Mater*., vol. 28, no. 12, pp. 2399–2407, 2016. doi: 10.1088/2053-1583/aa57fd.

[11] P. Giannozzi, S. Baroni, N. Bonini, M. Calandra, R. Car, C. Cavazzoni, D. Ceresoli, G. L. Chiarotti, M. Cococcioni, I. Dabo, A. Dal Corso, S. de Gironcoli, S. Fabris, G. Fratesi, R. Gebauer, U. Gerstmann, C. Gougoussis, A. Kokalj, M. Lazzeri, L. Martin-Samos, N. Marzari, F. Mauri, R. Mazzarello, S. Paolini, A. Pasquarello, L. Paulatto, C. Sbraccia, S. Scandolo, G. Sclauzero, A. P. Seitsonen, A. Smogunov, P. Umari, R. M. Wentzcovitch, A. D. Corso, S. Fabris, G. Fratesi, S. de Gironcoli, R. Gebauer, U. Gerstmann, C. Gougoussis, A. Kokalj, M. Lazzeri, L. Martin-Samos, N. Marzari, F. Mauri, R. Mazzarello, S. Paolini, A. Pasquarello, L. Paulatto, C. Sbraccia, S. Scandolo, G. Sclauzero, A. P. Seitsonen, A. Smogunov, P. Umari, and R. M. Wentzcovitch, "QUANTUM ESPRESSO: a modular and open-source software project for quantum simulations of materials.," *J. Phys. Condens. Matter*, vol. 21, no. 39, p. 395502, Sep. 2009. doi:10.1088/0953-8984/21/39/395502.

[12] A. A. Mostofi, J. R. Yates, G. Pizzi, Y.-S. Lee, I. Souza, D. Vanderbilt, and N. Marzari, "An updated version of wannier90: A tool for obtaining maximally-localised Wannier functions," *Comput. Phys. Commun*., vol. 185, no. 8, pp. 2309–2310, 2014. doi: 10.1016/j.cpc.2014.05.003.

[13] G. Bin Liu, W. Y. Shan, Y. Yao, W. Yao, and D. Xiao, "Three-band tight-binding model for monolayers of group-VIB transition metal dichalcogenides," *Phys. Rev. B - Condens. Matter Mater. Phys*., vol. 88, no. 8, p. 85433, 2013. doi: 10.1103/PhysRevB.88.085433.

[14] S. Datta, *Quantum Transport: Atom to Transistor*. Cambridge University Press, 2005. doi:10.1017/CBO9781139164313.